Gallium nitride deposition via magnetron sputtering: Linking plasma-surface interactions and thin film crystalline features

Lakshman Srinivasan, Kristaq Gazeli, Swaminathan Prasanna, Laurent Invernizzi, Pere Roca I Cabarrocas, Guillaume Lombardi, Karim Ouaras

Gallium Nitride Deposition via Magnetron Sputtering: Linking Plasma-Surface Interactions and Thin Film Crystalline Features

Lakshman Srinivasan[1,2], Kristaq Gazeli[3], Swaminathan Prasanna[3], Laurent Invernizzi[3], Pere Roca i Cabarrocas[1,2], Guillaume Lombardi[3], Karim Ouaras[1,a)]

AFFILIATIONS

[1] LPICM - CNRS, Ecole Polytechnique, Institut Polytechnique de Paris, Palaiseau 91128, France.

[2] IPVF, Institut Photovoltaïque d'Ile-de-France, 18 Bd Thomas Gobert, 91120 Palaiseau, France.

[3] LSPM - CNRS, Université Sorbonne Paris Nord, 99 Av. J. B. Clément, 93430 Villetaneuse, France.

[a)] Author to whom correspondence should be addressed: karim.ouaras@polytechnique.edu

Keywords – Gallium Nitride (GaN), Plasma, III-V Semiconductors, Thin films, Reactive Sputtering, Optical Emission Spectroscopy, Microwave interferometry, plasma surface interaction

Abstract

Ga-atoms dynamic in an Ar/N_2 magnetron sputtering discharge for GaN deposition is explored employing plasma diagnostic techniques such as optical emission spectroscopy and microwave interferometry. Through the assessment of gas temperature, electron temperature and density measured from the abovementioned diagnostics, we estimated both the flux and average energy of Ga-atoms impinging on the substrate. Emphasizing the working pressure as a pivotal factor, this study uncovers a correlation between the Ga-atoms flux, their average energy, and the growth rate and crystallinity of the GaN films extracted from ex-situ characterizations. Notably, the pressure value (6.6 Pa) at which both the growth rate and crystalline fraction are the greatest is also the condition at which both the flux and energy of Ga-atoms impinging on the target are maximal. The findings pave the way for improving the understanding and control of the complex interplay between plasma conditions and resulting film properties in the sputtering process.

1. Introduction

Gallium nitride (GaN), belonging to the family of wide bandgap semiconductors (3.4 eV), has attracted the interest of the scientific and industrial communities as it became a key material for devices that have to withstand higher voltages, frequencies and temperatures than Silicon[1)]. GaN is conventionally produced using growth technics such as molecular beam epitaxy Metal Organic Chemical Vapor Deposition (MOCVD)[2)], Hydride Vapor Phase Epitaxy (HVPE)[3)] or Molecular Beam Epitaxy (MBE)[4)]. Unfortunately, these technics require high operating temperatures (~800-1100 °C), which make them impractical for GaN deposition on thermally sensitive substrates for flexible devices *inter alia*. This may also cause strain issues and film cracking upon cooling[5)] when GaN is envisioned to be deposited in cheap substrates such as Silicon that has a lower thermal expansion coefficient than GaN (2.59×10^{-6} K^{-1} versus 5.59×10^{-6} K^{-1}, respectively). Therefore, it is desirable to develop processes operating at lower temperatures while respecting two criteria: (i) keep the high-quality standards offered by the counterpart methods, and (ii) reduce the cost associated to GaN production which currently constraints its utilization for niche applications.

Reactive magnetron sputtering, involving Ar/N_2 plasma facing a Ga target, has gained a lot of attention over the past few years[6)–8)]. This is because (i) it does not require ultra-high vacuum conditions such as MBE; (ii) it's a prime candidate for large-scale production; (iii) it eliminates the necessity of toxic or organic gases unlike MOCVD and (iv) it involves a highly reactive environment where ions and radicals contribute to the growth process while operating at temperatures as low as room temperature[9)]. Many publications have addressed the foundation of sputtering and growth mechanism theories to better understand the dynamics behind the interaction of ions and atoms with the surfaces using various simulation methods[10)]. Moreover, the transport of particles and deposition processes refer to a wide researched field [11),12)]. In sputtering discharges, parameters for growth optimization are manifold (working pressure, RF power, total gas flow, flow ratio…), and often strongly correlated. Most of the time, the impact of these parameters on the film quality, be it structural, electrical or optical, are evaluated on the final product after deposition using ex-situ measurements using solid-state diagnostics. However, studies that correlate the gas phase (e.g. transport of the sputtered atoms) with the properties of the grown film are scarce. For instance, if one considers the growth rate of a thin film and study its evolution as a function of any process parameter, it is somewhat intuitive that the flux of the sputtered atoms would allow making a rough estimation of the growth rate. However, it has rarely been comprehensively studied and related to the gas phase chemistry. Similarly, for low temperature deposition methods such as sputtering, producing a thin film with a high crystallinity and low density of defects is one of the most critical challenges that limits its widespread use. In most cases, crystallinity is only evaluated after the deposition process *via* x-ray diffraction (XRD) or high-resolution electron microscopy. If one only considers thin films, there are several studies relying on film analysis that relate the evolution of the crystalline structure with the variation of the process parameters[13)]. However, very few studies have linked the process parameters with the energy of the plasma-produced incoming atoms at the substrate for better understanding and controlling the crystallinity of the thin film. Therefore, as a way to bridge the gap between studies related to plasma phase and thin film analyses, especially for GaN that is lesser studied as far as plasma processes are concerned, we propose a study that aims at correlating the Ga-atoms from the gas phase to their interaction with the film surface and their impact on film features. For this purpose, we considered two parameters – the flux of Ga-atoms φ_{Ga} and the

average energy of the impinging Ga atoms at the substrate $\overline{E_{Ga}}$. These were calculated through the determination of the gas temperature T_{gas}, the electron temperature T_e and the electron density n_e using gas phase diagnostics described in the next section. In our previous work[14], we had shown that the pressure has the most influential impact on the crystalline quality of our GaN thin films. Hence, we focused here on the role of the operating pressure as the main parameter. In section 2, we describe the plasma reactor setup used for GaN thin film deposition, solid-state characterization as well as the relevant plasma diagnostics that were performed. In section 3, we elaborate on plasma characterizations performed to access the main plasma parameters mentioned before. By using these quantities, the flux and the average energy of the Ga-atoms were calculated using the methodology presented in section 0. In section 0, we correlate the experimental results of the films characterizations to that of Ga-atoms dynamics.

2. Experimental

The GaN deposition and plasma diagnostics were carried out in a custom-built RF magnetron sputtering reactor which is schematically shown in Figure 1.a and thoroughly described elsewhere[14]. The plasma was ignited thanks to a 2"-circular magnetron sputtering source (Torus® with standard magnet (S) configuration - Kurt J. Lesker Company) that houses a liquid gallium target exposed to an Ar/N_2 plasma (99.9999% Ar and N_2). The liquid Ga target layer was produced using melted Ga pellets (99.9999% purity - Alfa Aesar). For this purpose, the solid Ga pellets were introduced into a stainless steel crucible. The later was then heated to 50°C enabling the formation of continuous liquid Ga layer which was then solidified under RT conditions. Then, a pure Argon plasma was used before any deposition for cleaning the target using a shutter to protect the silicon substrate. The magnetron was powered by a 300 W RF generator (13.56 MHz) connected to an impedance matching box (TRUMPF PFG 300RF - Huttingter Elektronik). A vacuum base pressure of ~10^{-7} mbar was achieved in the process chamber thanks to a dry pump (nXDS-10iR scroll Pump) and a turbo-molecular pump (Alcatel ATP-900). The working pressure, which is the parameter that was investigated, was varied in the range 2.6 – 13.3 Pa. All the other operating conditions were kept constant, namely a total gas flow rate of 20sccm, an Ar/N_2 flow ratio of 3:2 and a RF power of 100 W. The depositions were done on 2-inches n-type c-Si (100) wafers without heating the substrate. In this study, we consider the growth rate and the crystalline fraction as the experimental reference data to be compared with the calculated data of both the flux of the ejected Ga-atoms (φ_{Ga}) and the average energy of impinging atoms to the substrate ($\overline{E_{Ga}^{sub}}$), respectively. The growth rate (Figure 1.b) was deduced from the thickness values that were extracted from cross-sectional images (Figure 1.a) acquired with a scanning electron microscope (Zeiss Merlin). In Figure 1.a, a HR-TEM top-surface image of a typical pc-GaN obtained at 13.3Pa is also shown. The crystalline fraction (Figure 1.c) was estimated from XRD spectra of the GaN samples (Figure 1.d) using Grazing Incidence (at 0.5°) X-ray diffraction (GIXRD) - Panalytical Empyrean Diffractometer (CuK_α) radiation (λ=1.5406 Å) - by calculating the ratio of the area of amorphous and crystalline peaks[15]. As far as plasma species are concerned, relevant plasma diagnostics were performed to generate the plasma quantities required for the calculation of φ_{Ga} and $\overline{E_{Ga}^{sub}}$, thanks to the equations introduced in section 4. The targeted plasma quantities were the gas temperature (T_{gas}), the electron temperature (T_e) and the electron density (n_e). Gas and electron temperatures were respectively estimated from rotational and electron excitation temperatures determined by Optical Emission Spectroscopy (OES). For gas temperature measurements, a high-resolution spectrometer (Jobin Yvon THR 1000; 1200 grooves/mm grating; 30 µm entrance slit width) backed with an intensified charge-coupled device (Princeton Instruments PI-MAX 3 1024i) was used. The electron excitation temperature was determined using a low-resolution (~0.3 nm) spectrometer (AVANTES Avaspec-ULS4096 CL-EVO; 10 µm entrance slit width) equipped with a wideband optical fiber (UV-VIS-IR; 200 µm core). The recorded spectra were spatially integrated and calibrated in terms of relative emission intensity using an adequate irradiance standard (OL FEL-M; 250-1100 nm). To determine the average value of the electron density, we used a commercial microwave interferometer (Miwitron 2650 MWI) that works at a frequency of 26.5 GHz[16].

3. Ar/N_2 plasma characterization

3.1. Rotational temperature of probe molecules as an estimate of the gas temperature

Ideally, in pure N_2 plasmas, when the excitation of N_2 from its ground state N_2(X) to the N_2(C) state occurs exclusively through electron impact, the rotational distribution of the N_2(C) level reflects that of the ground state. Thus, by also assuming the rotational distribution of the N_2(X) state to be in equilibrium with the translational motion of the neutral gas species (N_2), the rotational temperature T_{rot} of N_2(C) may be considered as a good estimate of that of the N_2(X). Hence, the T_{rot} determined from the second positive system SPS - N_2(C-B) can be used as a good estimation of the gas temperature ($T_{rot} \sim T_{gas}$)[17]. This is true for the first negative system FNS - N_2^+(B-X) as well, when also assuming a dominance of electron impact ionization[18]. However, when argon is present in the plasma, one cannot rely on the use of the N_2(C) for estimating T_{gas}. In this case, resonant energy transfer from argon metastable atoms (Ar^*) to ground state nitrogen N_2(X) leads to a population of high rotational levels of the N_2(C) state and an overestimation of the gas temperature[17]. For this reason, only the FNS emission was used to measure T_{rot} in this work to estimate T_{gas} from the corresponding value of T_{rot}. For a more rigorous investigation of the hypothesis $T_{rot} \sim T_{gas}$ in this case, we used two different methods to access the T_{rot} of N_2^+(B). First, we compared the experimental spectrum of N_2^+(B-X) with a synthetic spectrum generated using the massiveOES software[19].

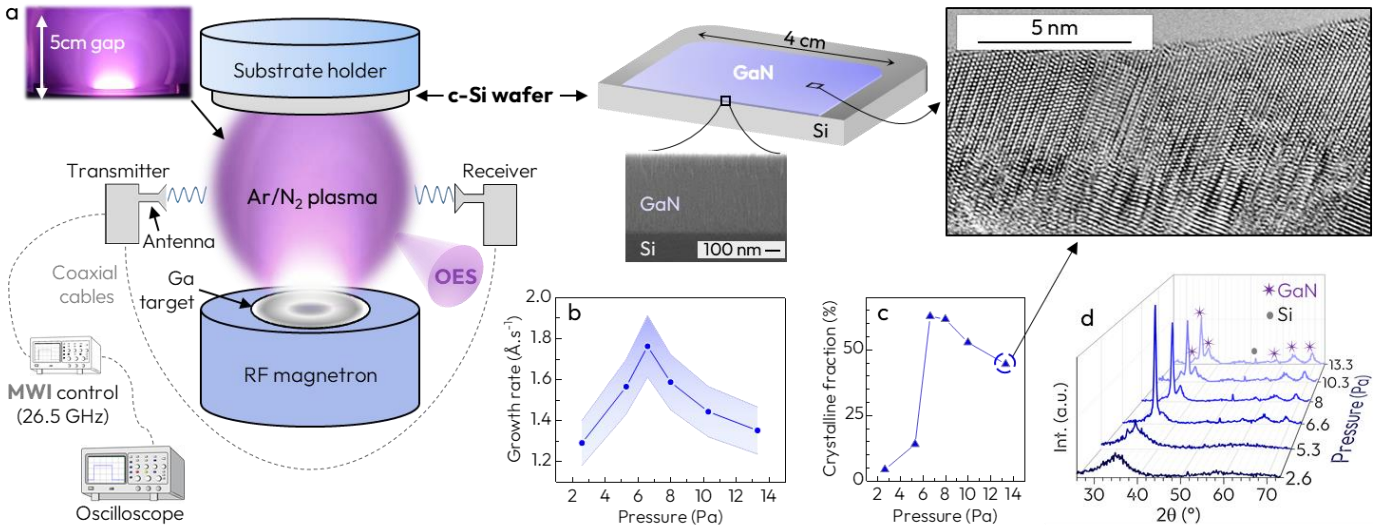

Figure 1. (a) Schematic of the plasma setup in which OES, MW interferometry and the cross-section SEM images of a typical GaN film are represented; (b-d) Growth rate, crystalline fraction and XRD spectra of the GaN films as a function of the pressure, respectively. Note: The background color from the graph in Figure 1.b represents the error bar.

In this approach, one rotational temperature is considered to generate the synthetic spectrum and achieve the best agreement with the experimental one. An example of the experimental spectrum and the single-band simulation is shown in Figure 2.a1, where the rotational temperature of N_2^+(B) was essentially obtained by comparing the experimental and synthetic line profiles of the emission band. The intensity of a rotational line from a rotational level J' in the upper vibronic state (v'), to a rotational level J'' in the lower vibronic state (v'') is expressed as[20]:

$$I(J',J'') = aS(J',J'')\exp(-E(J')/k_B T_{rot}) \quad (1)$$

where a is a constant that depends on the spectral response of the imaging system, $S(J',J'')$ is the line strength for each transition, $E(J')$ the rotational energy of the level J' and k_B the Boltzmann constant. Using the fitting method, a rotational temperature of ~445 ± 20 K was determined as shown in Figure 2.a1.

The second method was the Boltzmann plot by which T_{rot} was calculated from the slope of the line obtained through a linear regression of the experimental data as shown in Figure 2.a2:

$$\ln\left(\frac{I\lambda}{AG}\right) = B - \frac{E_k}{k_B T_{rot}} \quad (2)$$

where I denotes the intensity of a rotational line, A the transition probability, G the degeneracy of the upper level (statistical weight), λ the wavelength and E_k the rotational energy.

The advantage of this method over the previous one is that it can effectively discriminate different rotational temperatures which may be due to different production mechanisms of the probe molecule. Thus, one can inspect if the rovibronic emission is representative of one or more T_{rot} values. For example, at a working pressure of 6.6 Pa, T_{rot} was estimated to be in the range of ~467K ± 70K. This value is in relative agreement with that obtained in Figure 2.a1. Thus, the emission band may be described only with one rotational temperature. Indeed, in our conditions we do not expect any other mechanism to induce N_2 ionization besides electron impact. The small discrepancies in the temperature value measured by the two methods were integrated in the error bar of the gas temperature as a function of the pressure shown in Figure 2.a3. It can be seen that the gas temperature typically ranges from 350 – 520 K with some variations as the working pressure changes from 1.3 to 13.3 Pa. Notably, the highest temperature seems to be attained at 6.6 Pa.

3.2. Excitation temperature, electron temperature and electron density

The electronic excitation temperature T_{exc} reflects the distribution of electronic energy of excited states, achieved through collisions with electrons. In an ideal scenario, the energy distribution in these excited states can be described by the electron energy distribution function (EEDF), aligning T_e with T_{exc}. However, in non-equilibrium plasmas as the one studied here, where insufficient time exists for the electron distribution to equilibrate with the electronic excitation distribution, the reliability of the relationship $T_e \approx T_{exc}$ is questionable[21]. Currently, there are several discussions exploring the methods to estimate T_e in non-thermal plasmas[22)–24]. Yet, even assuming that the selected upper levels of atomic transitions are in local thermal equilibrium (LTE) and follow the Boltzmann statistics, T_{exc} would only provide a rough approximation of T_e, but it can at least provide an idea of the evolution of T_e as a function of the varying parameters of interest[25]. This information is particularly valuable in magnetron-based plasmas like ours where the use of Langmuir probes is impractical[26)–28]. Similar to the method used to determine the rotational temperature, the Boltzmann plot was used for the determination of the excitation temperature:

$$\ln\left(\frac{I_{ij}\lambda_{ij}}{g_i A_{ij}}\right) = -\frac{E_i}{k_B T_{exc}} + C \quad (3)$$

where I_{ij} is the relative intensity of the selected Ar-I emission line between levels i and j, λ_{ij} the wavelength in nm, g and A the statistical weight and the transition probability of a selected transition, respectively.

In this work, we used various argon emission lines to determine T_{exc}. Figure 2.b$_1$ and b$_2$ respectively show the emission spectra depicting the selected Ar-I lines and the associated Boltzmann-plot from which the slope of equation (3) was determined and used to extract T_{exc}. Overall, within the investigated pressure range, we found that T_{exc} varies from 3500 K to about 4200 K (Figure 2.b$_3$).

To estimate T_e, we mostly relied on values found in the literature as we did not have access to direct measurement of it. In RF magnetron sputtering systems similar to ours in terms of pressure and gas mixture, T_e ranges from ~1 to 2 eV[29),30)]. Then, to estimate its evolution as a function of the pressure, we assumed that T_{exc} would vary as same as T_e as for non-LTE plasma such as ours, which operates at a low pressure of a few Pa and which exhibits a low electron density (n_e~ 10^{10} cm^{-3}), 80% of the reactions are governed by direct excitation from the ground state[26)]. Figure 2.c shows the variation of T_e as a function of the pressure, the error bar being the same as that of T_{exc}. Typically, we assume that T_e values are in the range of ~1.2 to 1.8 eV for pressures varying from 1.3 to 13.3 Pa.

A far as electron density is concerned, it was directly determined using MWI (Figure 2.d). We should mention that these values are line-of-site-integrated along the path of the microwave traveling the discharge.

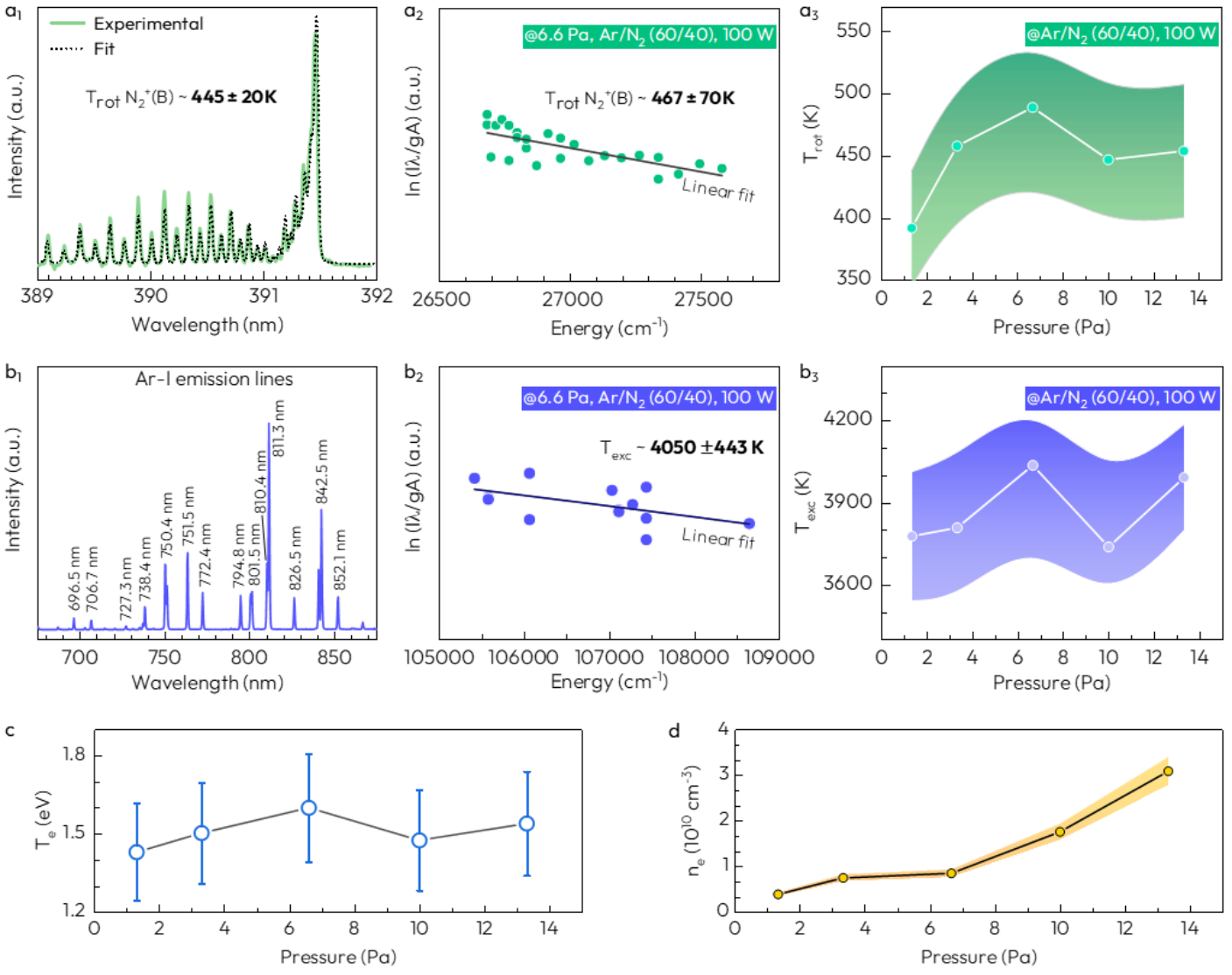

Figure 2. Rotational spectrum of the FNS of N_2^+ (a$_1$); Boltzmann plot of the experimental rotational spectra (a$_2$); Evolution of the estimated gas temperature of N_2^+(B) as a function of the working pressure (a$_3$); Ar-I emission lines from the OES spectra in Ar/N_2 plasma (b$_1$); Boltzmann plot of the corresponding lines from the emission spectra (b$_2$); evolution of the estimated excitation temperature as a function of the working pressure (b$_3$); Evolution of the electron temperature estimated from the excitation temperature values as a function of the pressure (c) and Evolution of the average electron density measured with microwave interferometry as a function of the pressure (d). The operating conditions were: RF power – 100W and Ar/N_2 (3:2) at a total flow of 20 sccm. Note: The background color from the graph in Figure 2.a$_3$, b$_3$ and d represents the error bar.

Overall, within the pressure range between 1.3 and 13.3 Pa, it appears that n_e varies from ~0.4×10^{10} cm^{-3} to ~3 ×10^{10} cm^{-3}. Finally, by determining the values of the T_{gas}, T_e and n_e at the same pressure values at which thin films deposition was carried out, we have the necessary data to estimate the flux and the average energy of the sputtered Ga atoms reaching the substrate.

4. Estimating Ga-atoms flux and average energy

To estimate the Ga-atoms flux φ_{Ga} and energy E_{Ga}^{sub} in the investigated sputtering process that involves Ar and N_2 as process gases and Ga as target, we made the following assumptions:

– We only considered Ar^+ and N_2^+ as major ion species contributing to the sputtering of Ga. Ideally, for modeling a N_2-based plasma sputtering process, N_2^+, N^+ and N^0 species have to be considered. However, it has been shown that, under conditions similar to ours, the dominant species are N_2^+ ions[31].

– The incident Ar^+ and N_2^+ ions at the target as well as the sputtered Ga atom are all normal to the target surface.

– The sputtered Ga-atoms are neutral, in the ground state, and only collide elastically with neutral Ar background gas. This assumption was made because of the lack of data regarding the interaction potential of Ga-atoms with molecular N_2 gas. This assumption is commonly considered for most of plasma modelling investigations carried out for Ar-N_2 plasma discharges[12].

– The energy losses of sputtered Ga-atoms from the target to the substrate occur only in a pathway normal to the substrate's surface without accounting for angular effects[32].

In addition to these general assumptions, we also made some specific assumptions, which will be detailed hereafter.

4.1. Ga-atoms flux (φ_{Ga})

To determine φ_{Ga}, the flux of Ar^+ and N_2^+ ions hitting the Ga target φ_i and their respective sputter yields $Y(E)$ were required. The sputtering yield $Y(E)$ of the Ga atoms was calculated using Bohdansky's empirical formula[33], knowing the incident ion energies E:

$$Y(E) = 0.0064\,.\,M_2\,.\,\gamma^{\frac{5}{3}}\,.\,E_s^{\frac{1}{4}}\,.\left(1-\frac{E_{th}}{E}\right)^{\frac{7}{2}} \qquad (4)$$

where $\gamma = \frac{4M_1M_2}{(M_1+M_2)^2}$ is the energy transfer factor in a direct collision, M_1 and M_2 the masses of the incident ion (Ar^+ or N_2^+) and the target material (Ga) respectively, E_{th} the threshold energy equal to $8E_s/\left(M_1/M_2\right)^2$, E_s the surface binding energy of Ga atoms (~2.8 eV)[34].

For instance, at an incident ion energy of 700 eV (corresponding to the typical value of the DC self-bias on our target), the Ga sputtering yield $Y(E)$ calculated from equation (4) for Ar^+ is ~2.4 Ga atoms/ion and for a N_2^+ ion is ~1.5 Ga atoms/ion (Figure 3). Once the sputter yield known, φ_i was determined based on the assumption of a collision-less sheath model[35]. In a collision-less sheath, φ_i is the product of the plasma density at the sheath edge n_s and the minimum velocity of the ions v_{Bohm} at the sheath edge (Bohm velocity)[35] following the Child-Langmuir theory [36].

$$\varphi_i = n_s v_{Bohm} = \frac{4}{9}\epsilon_0\left(\frac{2e}{M}\right)^{1/2}\frac{{V_0}^{3/2}}{s^2} \qquad (5)$$

where V_0 is the difference of potential between the plasma and the cathode, e the electron charge, M the ion mass, ϵ_0 the electrical permittivity in free space and $s = \frac{\sqrt{2}}{3}\lambda_{DS}\left(\frac{2V_0}{T_e}\right)^{3/4}$ the sheath thickness where $\lambda_{DS} = \left(\epsilon_0 T_e/en_s\right)^{1/2}$ corresponds to the Debye length.

Assuming the quasi-neutrality in the bulk ($n_e \sim n_i$) and that the plasma density at the sheath edge can be calculated by substituting the Bohm Potential into Boltzmann's equations for electrons, we considered n_s~0.61 n_e [37].

Overall, knowing T_e and n_e from OES (Figure 2.c) and MWI interferometry measurements (Figure 2.d) respectively, we estimated φ_i using equation (5). The ratio of the flux of the Ar^+ and N_2^+ was determined taking into account their partial pressures[12].

Finally, by multiplying the ion fluxes with the sputter yield $Y(E)$ from equation (4), we got the flux of the Ga atoms sputtered from the target (φ_{Ga}):

$$\varphi_{Ga} = \left(\varphi_{Ar^+} * Y(E)_{Ar^+\to Ga}\right) + \left(\varphi_{N_2^+} * Y(E)_{N_2^+\to Ga}\right) \qquad (6)$$

4.2. Ga-atoms energy at the substrate (E_{Ga}^{sub})

Once the Ga-atoms are sputtered, they undergo several collisions before reaching the substrate. An important parameter to consider here is the sputtered atom energy distribution function (EDF) since it describes the initial energy with which the Ga atoms travel the path from target to substrate. To estimate it, we considered a Thompson energy distribution function[38] :

$$F(E) \propto \frac{1-\left(\frac{E_s+E}{\gamma E_i}\right)^{\frac{1}{2}}}{E^2\left(1+\frac{E_s}{E}\right)^3} \quad , E < \gamma E_i - E_s \qquad (7)$$

where E is the energy of the sputtered atom, E_s the surface binding energy of target's atoms and E_i the incident ion energy.

In the case of Ga, the sputtered atoms should have a minimum energy slightly above their surface binding energy (~2.8 eV) and the maximum energy which can be as high as the incident ion energy ~γE_i[39], i.e. 700 eV.

In Figure 4, the Thomson distribution of the sputtered Ga atoms is plotted for the particular conditions considered in the present work, namely Ar^+ and N_2^+ ions at 700 eV. The average energy of the sputtered atoms, $\overline{E_{Ga}}$ can be calculated by correlating the Thompson distribution function of the sputtered Ga atoms with the Sigmund distribution function[40].

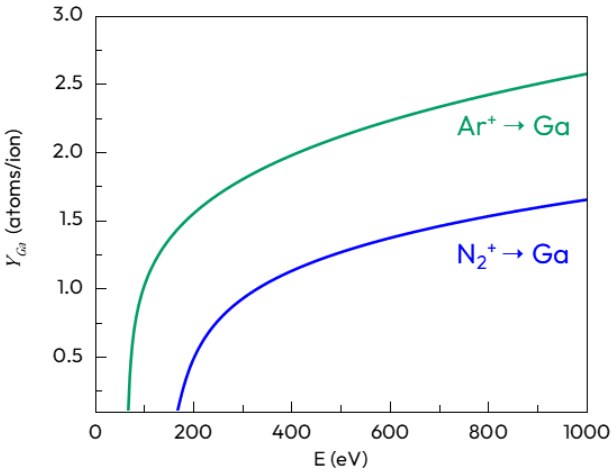

Figure 3. Calculated sputtering yield, $Y(E)$ of Ga by Ar^+ and N_2^+ considering Bohdansky's empirical formula[33].

By adopting simplifications for which methodologies and calculations are elaborated in literature[41)42)], the following equation was used to calculate $\overline{E_{Ga}}$:

$$\overline{E_{Ga}} = 2E_s \ln\left(\frac{\gamma E_i}{E_s}\right) - 3E_s \qquad (8)$$

In our case, $\overline{E_{Ga}}$ would be around ~17 eV/atom and ~22 eV/atom for Ar^+ and N_2^+ respectively. For the sake of comparison, the theoretical values derived from simulations performed by SRIM/TRIM (stopping/transport range in ions and matter)[32] gave value of ~16 eV/atom and ~23 eV/atom for Ar^+ and N_2^+ ions, respectively.

As mentioned above, the sputtered Ga atoms will suffer from collisions with the ambient gas so losing a part of their kinetic energy, thus modifying their EDF which does not follow a Thompson's distribution anymore[33]. To calculate the Ga-atoms energy at the substrate $\overline{E_{Ga}^{sub}}$, an analytical approach was employed, which considers the energy loses along a pathway normal to substrate (without accounting for angular effects)[11),32),43)]. The average kinetic energy at a distance d from the target is given by:

$$\overline{E_{Ga}^{sub}} = \left(\overline{E_{Ga}} - k_B T_{gas}\right)\left[\frac{E_f}{E_i}\right]^n + k_B T_{gas} \qquad (9)$$

where $\frac{E_f}{E_i}$ = 1- $\gamma/2$ the kinetic energy ratio after and before a collision, $n = dP\tau/k_B T_{gas}$ the number of collisions along the path, d the distance between the target and the substrate (~5 cm), P and T_{gas} the sputtering gas pressure and temperature respectively, and τ the collisional cross-section, assuming hard-core interactions[11].

The collisional cross-section for the interaction of Ga atoms with an Ar ion is scarcely found in literature. As τ mainly depends on the interatomic distance, the mass and the number of collisions[44], we therefore assumed its value to be that adopted for the couple copper (Cu)/Ar (~2.5×10^{-19} m^2) as the mass number and the inter-atomic distance of Cu are very close to that of Ga.

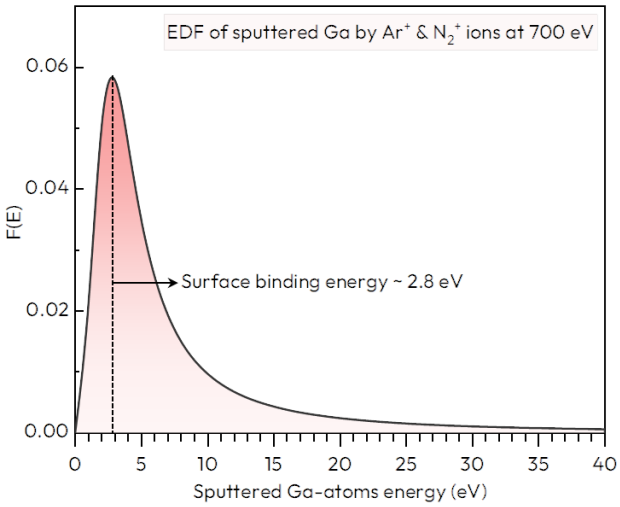

Figure 4. Thompson energy distribution function (EDF) of sputtered Ga atoms by Ar^+ and N_2^+ ions calculated at a kinetic energy of 700 eV.

Moreover, the interaction of Cu/Ar has been widely studied for sputtering model[43]. Finally, the average kinetic energy of the Ga atoms impinging at the substrate was estimated using the gas temperature T_{gas} measured by OES (Figure 2.a3).

5. Correlation between gas phase and thin film properties

Figure 5 illustrates the variation of four different parameters that can be distinguished in two categories: (i) those that were determined experimentally by probing the grown films, namely the growth rate (Figure 5.a) and crystalline fraction (Figure 5.b) and (ii) those determined by calculation using experimental values acquired from the gas phase (T_{gas}, T_e, n_e), namely φ_{Ga} (Figure 5.c) and $\overline{E_{Ga}^{sub}}$ (Figure 5d).

The pressure range in Figure 5 was the one at which the growth was performed, i.e. 2.6-13.3 Pa. By comparing the changes observed in growth rates (Figure 5.a) and those of the flux of Ga atoms reaching the substrate (Figure 5.c), a similar trend is observed all over the pressure range. Indeed, an increase of both parameters can be seen as the pressure rises from 2.6 to 6.6 Pa, the growth rate and φ_{Ga} increasing from 1.2 Å/s to 1.9 Å/s and from 0.2×10^{15} to 1.2×10^{15} $cm^{-2}.s^{-1}$, respectively. Notably, the pressure value of 6.6 Pa corresponds to the maximal value for both parameters after which both experience a decrease. This trend may be explained through two effects:

i) when pressure increases up to a certain extent, 6.6 Pa in our case, the mean-free path of the species overall decreases due to more frequent collisions between Ar and electrons, enhancing the production of Ar^+ ions that bombard the target and consequently increasing the sputtered Ga-atoms flux[45]

ii) beyond 6.6 Pa, the growth rate tends to drop which could be related to an increase of Ga-atoms collisions and therefore fewer atoms reaching the substrate, implying a reduction of the growth rate[46]. Moreover, electrons lose more

energy trough collisions with Ar leading to their excitation, hence less electrons are available for direct ionization of Ar.

These hypotheses remain unconfirmed as our flux calculations assume interactions perpendicular to the surface. However, even if several assumptions were made to determine φ_{Ga}, it happens that the estimation of the growth rate from the calculated values is in a good agreement with experimental data. For example, if one considers an hexagonal wurtzite GaN structure such as ours, the number of atoms in 1 cm^3 is ~8.9×10^{22} [47]. At 6.6 Pa which corresponds to φ_{Ga}~ 1.1 x 10^{15} $cm^{-2}s^{-1}$, we obtained a growth value of ~2.4 Å/s, which is quite similar to the experimental value, i.e. ~1.9 Å/s. Note that this deviation might be due to the variation in the flux of N-atoms at the substrate or some contaminants present in the lattice structure. It is worth to note that the increase in growth rate between 2 and 6 Pa is almost doubled while the Ga flux increases by four times.

Therefore, by using this approach, we demonstrate that the Ga-atoms flux can be a useful indicator to get the trend in the growth rate of GaN. Interestingly, the pressure at which the growth rate is maximal (6 Pa) also coincides with the maximal crystalline fraction (Figure 5.b). In the well-known Thronton's zone model[48], the working pressure is considered as one of the most important parameters as far as the film quality is concerned. Indeed, varying the pressure indirectly has an effect on the kinetic energy of both impinging ions at the target and atoms arriving at the substrate. The energy of atoms/ions impinging on the substrate is crucial as it affects the mobility of adatoms at the surface. This mobility is a key driver in the formation of crystallites, which are defined by energy planes during the processes of nucleation and coalescence[49]. When comparing the variation in $\overline{E_{Ga}^{sub}}$(Figure 5.d) as a function of the working pressure with that of the F_C (Figure 5.b), a similar pattern can be seen. As the pressure increases from 2.3 to 6.6 Pa, $\overline{E_{Ga}^{sub}}$ rises, leading to the enhancement of the mobility of adatoms, which in turn boosts the crystalline fraction. The thin films of GaN grown at pressure below 6.6 Pa, exhibit an F_C value of a 5-10 % so are deemed amorphous, evidenced by broad peaks from GXRD (Figure 1.d). Increasing the pressure to 6.6 Pa transitions the film from an amorphous to a polycrystalline structure with an F_C of ≈60%. This is associated to an increase in the $\overline{E_{Ga}^{sub}}$ value (Figure 5.d). Furthermore, beyond 6.6 Pa, F_C decreases from ≈60% to ≈40%. Although being not of a similar linearity than F_C, $\overline{E_{Ga}^{sub}}$ follows a decreasing trend where at 13.3 Pa, the $\overline{E_{Ga}^{sub}}$ decreases back to resemble values close to the ones observed for amorphous samples (2.3 Pa), despite the film being polycrystalline. This could be reasoned by i) surface interactions - the increased availability of nitrogen precursors at higher pressures, that might facilitate the nucleation and growth of crystalline domains on the surface, ii) sputtering dynamics of our model only assumes the interactions with Ar species in the discharge (not N-related species). Therefore, increased pressure can lead to enhanced scattering and collisions between sputtered atoms and background gas molecules such as N_2.

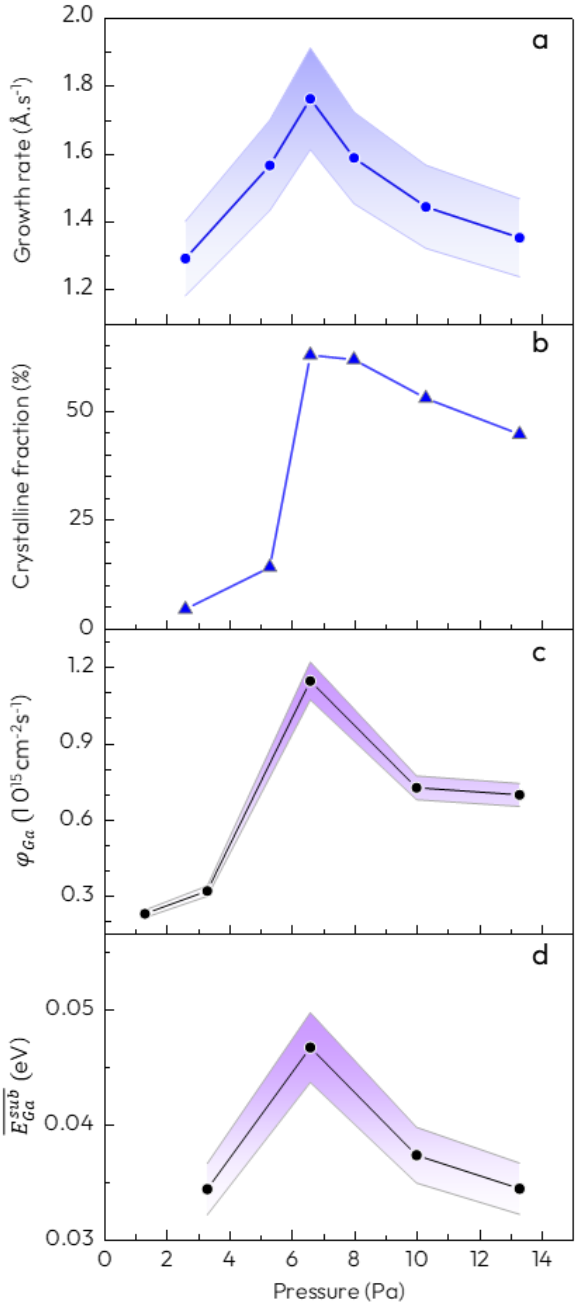

Figure 5. Growth rate (a), Crystalline fraction (b), flux of Ga-atoms ejected from the target (c) and average energy of Ga-atoms reaching the substrate (d) as a function of pressure. The operating conditions were: RF power – 100W and Ar/N_2 (3:2) at a total flow of 20 sccm.

This can result in reduced energy transfer to the sputtered Ga atoms, leading to a relatively lower average energy despite the presence of polycrystalline structures. Barring the anomaly, the correlation suggests that the average energy of the sputtered Ga atoms reaching the substrate is closely linked to influencing the initial stages of film growth and can be associated with the improvement/degradation of the crystalline quality of the GaN film. In the following studies, further experiments will be carried out to correlate other process parameters such as the RF power and the partial pressure of the sputtering gas (Ar/N_2) with the flux and the average energy of Ga atoms toward a better control of the deposition process.

6. Conclusion

In this study we used plasma diagnostic techniques, specifically optical emission spectroscopy (OES) and microwave interferometry (MWI) to investigate the dynamics of Ga-atoms for the specific case of Ar/N_2 sputtering discharge used for GaN deposition. By estimating the gas temperature and both electron temperature and density, we were able to estimate both the flux and the average energy of sputtered Ga atoms impinging on the substrate. Our study primarily focused on the impact of varying pressure as a critical process parameter, and its subsequent influence on these plasma characteristics. The investigation revealed that, within a pressure range of 1-15 Pa, the flux of Ga atoms is in the range of ~2×10^{14} - 1×10^{15} $cm^{-2}s^{-1}$. Notably, the average energy of the sputtered Ga atoms is contingent on the type of incident ions, be it Ar^+ or N_2^+, with an initial value of approximately 20 eV/atom. However, there is a significant energy loss observed for Ga atoms travelling from the target to the substrate, resulting in an average energy at the substrate of around 0.05 eV/atom. A key aspect of this study was the correlation between the flux and the average energy of the Ga atoms with the growth rate and crystallinity of the deposited film, as a function of varying pressure. We observed that the Ga atom flux serves as a reliable indicator of the trends in growth rate of GaN. More importantly, the average energy at the substrate exhibited a direct correlation with the crystalline fraction of the GaN film. The highest quality film in terms of growth rate and crystalline fraction was deposited at pressure of 6.6 Pa, highlighting the significance of this parameter. Building on these findings, future research will extend to examining how these parameters vary with other process variables, such as gas flow rates and RF power adjustments. We aim to understand the complex interplay between plasma conditions and the resultant film properties, thereby refining our understanding and control of the sputtering process.

Acknowledgements

This work was funded by the French National Research Agency trough contract No. ANR-22-CE51-0011-01 (GASPE project) and No. ANR-IEED-002-01. Authors would like to thank the MITI-CNRS - "Réseau des Plasmas Froids" for providing the MWI. We are grateful to Marc Malvaux for his help with reactor's transportation from LPICM to LSPM, Cédric Noël for the MWI installation and Nicolas Fagnon for his help with reactor's installation.

AUTHOR DECLARATIONS

Conflict of Interest

The authors have no conflicts to disclose.

Author Contributions

Lakshman Srinivasan: Investigation (lead); Formal analysis (equal); Conceptualization (equal); Methodology (equal); Visualization (supporting); Writing – original draft (equal); Writing – review & editing (equal). **Kristaq Gazeli:** Supervision (supporting); Investigation (equal); Methodology (equal); Formal analysis (equal); Writing – review & editing (equal). **Swaminathan Prasanna:** Investigation (supporting); Methodology (equal); Writing – review & editing (equal). **Laurent Invernizzi:** Investigation (supporting); Writing – review & editing (equal). **Pere Roca i Cabarrocas:** Supervision (equal); Writing – review & editing (equal). **Guillaume Lombardi:** Supervision (equal); Project administration (equal); Writing – review & editing (equal). **Karim Ouaras:** Investigation (supporting); Methodology (equal); Conceptualization (equal); Visualization (equal); Writing – original draft (equal); Writing – review & editing (equal). Supervision (lead); Funding acquisition (equal); Project administration (equal).

Data availability

The data that support the findings of this study are available from the corresponding authors upon reasonable request.

References

1) A. A. Burk Jr, M. J. O'loughlin, R. R. Siergiej, A. K. Agarwal, S. Sriram, R. C. Clarke, M. F. MacMillan, V. Balakrishna and C. D. Brandt, Solid-State Electron. **43** [8], 1459 (1999).
2) H. Amano, I. Akasaki, K. Hiramatsu, N. Koide and N. Sawaki, Thin Solid Films **163**, 415 (1988).
3) K. Fujito, K. Kiyomi, T. Mochizuki, H. Oota, H. Namita, S. Nagao and I. Fujimura, Phys. Status Solidi A **205** [5], 1056 (2008).
4) K. A. Bertness, A. Roshko, L. M. Mansfield, T. E. Harvey and N. A. Sanford, J. Cryst. Growth **310** [13], 3154 (2008).
5) A. Krost and A. Dadgar, Phys. Status Solidi A **194** [2], 361 (2002).
6) E. C. Knox-Davies, J. M. Shannon and S. R. P. Silva, J. Appl. Phys. **99** [7], 073503 (2006).
7) F. Mu, R. He and T. Suga, Scr. Mater. **150**, 148 (2018).
8) C. M. Furqan, J. Y. Ho and H. S. Kwok, Surf. Interfaces **26**, 101364 (2021).
9) J. T. Gudmundsson and D. Lundin, in *High Power Impulse Magnetron Sputtering*, eds. D. Lundin, T. Minea and J. T. Gudmundsson (Elsevier, 2020) pp. 1.
10) D. Depla and S. Mahieu, *Reactive sputter deposition* (Springer, 2008) Vol. 109.
11) P. Brault, A.-L. Thomann and M. Cavarroc, Eur. Phys. J. D **77** [2], 19 (2023).
12) S. Mahieu and D. Depla, J. Phys. Appl. Phys. **42** [5], 053002 (2009).
13) P. Losbichler and C. Mitterer, Surf. Coat. Technol. **97** [1–3], 567 (1997).
14) L. Srinivasan, C. Jadaud, F. Silva, J.-C. Vanel, J.-L. Maurice, E. Johnson, P. Roca i Cabarrocas and K. Ouaras, J. Vac. Sci. Technol. Vac. Surf. Films **41** [5], 053407 (2023).
15) G. E. Abrosimova, A. S. Aronin and N. N. Kholstinina, Phys. Solid State **52**, 445 (2010).
16) K. Ouaras, G. Lombardi, L. Couëdel, C. Arnas and K. Hassouni, Phys. Plasmas **26** [2], 023705 (2019).
17) S. Kasri, L. William, X. Aubert, G. Lombardi, A. Tallaire, J. Achard, C. Lazzaroni, G. Bauville, M. Fleury and K. Gazeli, Plasma Sources Sci. Technol. **28** [3], 035003 (2019).
18) K. Gazeli, P. Svarnas, B. Held, L. Marlin and F. Clément, J. Appl. Phys. **117** [9], 093302 (2015).

19) J. Voráč , L. Kusýn and P. Synek, Rev. Sci. Instrum. **90** [12], 123102 (2019).
20) J.-S. Poirier, P.-M. Bérubé, J. Muñoz, J. Margot, L. Stafford and M. Chaker, Plasma Sources Sci. Technol. **20** [3], 035016 (2011).
21) J. A. M. Van der Mullen, Phys. Rep. **191** [2–3], 109 (1990).
22) A. Yanguas-Gil, J. Cotrino and A. R. González-Elipe, Phys. Plasmas **11** [12], 5497 (2004).
23) D. Mariotti, Y. Shimizu, T. Sasaki and N. Koshizaki, J. Appl. Phys. **101** [1], 013307 (2007).
24) D. Mariotti, Y. Shimizu, T. Sasaki and N. Koshizaki, Appl. Phys. Lett. **89** [20], 201502 (2006).
25) F. J. Gordillo-Vázquez, M. Camero and C. Gómez-Aleixandre, Plasma Sources Sci. Technol. **15** [1], 42 (2005).
26) A. Kais, J. Lo, L. Thérèse and Ph. Guillot, Phys. Plasmas **25** [1], 013504 (2018).
27) Y. T. Lin, IEEE Trans. Plasma Sci. **47** [2], 1134 (2018).
28) R. Jaafarian and A. Ganjovi, Indian J. Phys. **93** [6], 799 (2019).
29) B. Fritsche, T. Chevolleau, J. Kourtev, A. Kolitsch and W. Möller, Vacuum **69** [1–3], 139 (2002).
30) I. Petrov, A. Myers, J. E. Greene and J. R. Abelson, J. Vac. Sci. Technol. Vac. Surf. Films **12** [5], 2846 (1994).
31) W. Möller and D. Güttler, J. Appl. Phys. **102** [9], 094501 (2007).
32) K. Meyer, I. K. Schuller and C. M. Falco, J. Appl. Phys. **52** [9], 5803 (1981).
33) J.-H. Hsieh and C. Li, Jpn. J. Appl. Phys. **42** [Part 1, No. 8], 5295 (2003).
34) Y. Kudriavtsev, A. Villegas, A. Godines and R. Asomoza, Appl. Surf. Sci. **239** [3–4], 273 (2005).
35) H.-B. Valentini, Phys. Plasmas **3** [4], 1459 (1996).
36) A. Palmero, E. D. Van Hattum, W. M. Arnoldbik and F. Habraken, Surf. Coat. Technol. **188**, 392 (2004).
37) H. S. Butler and G. S. Kino, Phys. Fluids **6** [9], 1346 (1963).
38) M. Kaminsky, Ed., *Radiation Effects on Solid Surfaces* (AMERICAN CHEMICAL SOCIETY, WASHINGTON, D. C., 1976) Vol. 158.
39) N. Mahne, M. Čekada and M. Panjan, Coatings **13** [8], 1448 (2023).
40) P. Sigmund, Phys. Rev. **184** [2], 383 (1969).
41) N. Mahne, M. Čekada and M. Panjan, Coatings **12** [10], 1541 (2022).
42) J. P. Biersack and W. Eckstein, Appl. Phys. Solids Surf. **34** [2], 73 (1984).
43) A. Gras-Marti and J. A. Valles-Abarca, J. Appl. Phys. **54** [2], 1071 (1983).
44) A. Palmero, E. D. van Hattum, H. Rudolph and F. H. P. M. Habraken, J. Appl. Phys. **101** [5], 053306 (2007).
45) S. Lin, J. Zhang, R. Zhu, S. Fu and D. Yun, Mater. Res. Bull. **105**, 231 (2018).
46) A. Büttner, A.-C. Probst, F. Emmerich, C. Damm, B. Rellinghaus, T. Döhring and M. Stollenwerk, Thin Solid Films **662**, 41 (2018).
47) A. Denis, G. Goglio and G. Demazeau, Mater. Sci. Eng. R Rep. **50** [6], 167 (2006).
48) J. A. Thornton, J. Vac. Sci. Technol. Vac. Surf. Films **4** [6], 3059 (1986).
49) I. Petrov, F. Adibi, J. E. Greene, L. Hultman and J.-E. Sundgren, Appl. Phys. Lett. **63** [1], 36 (1993).